ECS Transactions, 66 (5) 233-240 (2015)
10.1149/06605.0233ecst ©The Electrochemical Society

Variation of Spin Lifetime with Spin Injection Orientation in Strained Thin Silicon Films

J. Ghosh, D. Osintsev, V. Sverdlov, and S. Selberherr

Institute for Microelectronics, TU Wien,
Gußhausstraße 27-29/E-360, 1040 Wien, Austria

Spintronics attracts at present much interest because of the potential to build novel spin-based devices which are superior to charge-based microelectronic elements. Silicon, the main element of microelectronics, is promising for spin-driven applications. Understanding the peculiarities of the subband structure and details of spin propagation in thin silicon films in the presence of the spin-orbit interaction is under scrutiny. We show that shear strain has a strong influence in modifying the subband structure and thus can dramatically boost both of the surface roughness and electron-phonon interaction limited spin lifetime in an ultra-thin silicon-on-insulator-based transistor. We also report that a change in the spin injection direction has an impact on the spin lifetime.

Introduction

Growing technological challenges and increasing costs are gradually guiding MOSFET scaling to an end, which drives the search for alternative technologies as well as computational principles based on electron spin. Using electron spin may help to reduce power consumption and increase the computational speed of modern electronic circuits (1). Silicon is the primary material for microelectronics and can be used in building spin-driven applications. Silicon is composed of nuclei with predominantly zero magnetic moment, and the long spin lifetime in silicon is a consequence of the weak spin-orbit interaction (2). Since silicon technology is well established, it will help bringing silicon spin-driven devices to the market. Combined with the potentially easy integration with CMOS technology, silicon spintronic devices are expected to be faster and more compact. A number of novel spintronic devices has already been proposed (3).

As of the paramount importance of SOI and FinFET 3D technology for technology nodes from the 22nm to the 14nm nodes and beyond, spin lifetime in such structures is a very relevant issue under inspection. The lower estimate for the spin lifetime at room temperature obtained with a three-terminal injection scheme is of the order $0.1 - 1$ns (4). A long spin transfer distance of conduction electrons has been shown experimentally (5), hence spin propagation at such distances combined with a possibility of injecting spin at room (6) or even at elevated (7) temperature makes the fabrication of spin-based switching devices quite plausible in the near future. Besides, a large experimentally observed spin relaxation in electrically-gated silicon structures could become an obstacle in realizing spin-driven devices (2). Henceforth, a deeper understanding of the fundamental spin relaxation mechanism in silicon MOSFETs is

urgently required. Shear strain has traditionally been used to boost electron mobility, and a several orders of magnitude enhancement of spin lifetime in (001) oriented films subjected to [110] uniaxial tensile stress has also been predicted (8). Here we depict a further enhancement of the spin lifetime depending on the spin injection direction.

In bulk silicon the conduction electrons are positioned close to the minima of the three pairs of valleys near the edges of the Brillouin zone along the *X*-, *Y*-, and *Z*-axes. Each state is described by the valley index, the wave vector **k** relative to the valley minimum, and the spin orientation (spin-up and spin-down) on a chosen axis. The main mechanism of spin relaxation in bulk silicon is due to the f-phonons mediated electron transitions between the spin-up and down states located in the different valley pairs (9, 10). Uniaxial [001] stress removes the degeneracy between the *X*(*Y*)- and *Z*-valleys, and it is thus predicted to boost spin lifetime by a factor of three in bulk silicon (10). In (001) thin silicon films the confinement leads to the formation of an unprimed subband ladder from the *Z*-valleys and a prime ladder from the *X*(*Y*)-valleys. Due to the difference in the quantization energies the f-processes between the unprimed and primed subbands are suppressed even in unstrained films (11). Thus, spin relaxation due to the intra- and intersubband transitions between the states with opposite spin projections within the unprimed ladder must be considered.

A perturbative **k·p** approach is suitable to describe the electron subband structure in the presence of strain (12, 13). We use a spin-dependent **k·p** Hamiltonian considering only the relevant [001] oriented valleys, written at the vicinity of the X-point along the Z-axis in the Brillouin zone (13). The spin-orbit term couples the states with the opposite spin projections from the opposite valleys (12). This can produce a large mixing of the up(down)-spin states between the two unprimed degenerate subbands, resulting in spin hot spots characterized by strong spin relaxation. The condition for the hot spot is $(D\varepsilon_{xy} - \frac{p_x p_y}{M}) = 0$, where D is the shear deformation potential, $M^{-1} = m_t^{-1}\text{-}m_e^{-1}$ (cf. Table I), ε_{xy} is the applied shear strain, and (p_x, p_y) signify the projections of the in-plane momentum (13). The shear strain can lift the degeneracy between the unprimed subbands, which substantially improves the spin lifetime.

When the spin injection direction is changed, the hot spot spin precession is influenced which eventually further modifies the spin lifetime.

TABLE I. Parameter List

Parameters	Value	Unit
Spin-orbit term (7), Δ_{SO}	1.27	meVnm
Silicon electron rest mass, m_e	$9.1093 \cdot 10^{-31}$	Kg
Transversal effective mass, m_t	$0.19 \cdot m_e$	Kg
Longitudinal effective mass, m_l	$0.91 \cdot m_e$	Kg
Shear deformation potential, D	14	eV
Lattice constant, a	$5.431 \cdot 10^{-10}$	m
Position of the valley minimum relative to the *X*-point in unstrained silicon, k_0	$0.15 \cdot 2\pi/a$	m^{-1}

The Model

The effective Hamiltonian for electrons reads

$$H = \begin{bmatrix} H_1 & H_3 \\ H_3^{\dagger} & H_2 \end{bmatrix} \quad [1]$$

with H_1, H_2, H_3 are given by

$$H_j = [\frac{\hbar^2 k_z^2}{2m_l} + \frac{(-1)^j \hbar^2 k_0 k_z}{m_l} + \frac{\hbar^2(k_x^2+k_y^2)}{2m_t} + U(z)]\, I \quad [2]$$

$$H_3 = \begin{bmatrix} D\varepsilon_{xy} - \frac{\hbar^2 k_x k_y}{M} & (k_y - k_x i)\Delta_{SO} \\ (-k_y - k_x i)\Delta_{SO} & D\varepsilon_{xy} - \frac{\hbar^2 k_x k_y}{M} \end{bmatrix}, \quad [3]$$

where j = 1, 2, and I is the identity 2x2 matrix, and $\mathbf{k}=\mathbf{p}/\hbar$. The confinement potential is denoted by $U(z)$.

In order to find the subband wave functions and the subband energies it is convenient to perform a unitary transformation on the Hamiltonian

$$H = \begin{bmatrix} H_1' & H_3' \\ H_3' & H_2' \end{bmatrix}, \quad [4]$$

where the components will be written as

$$H_{1,2}' = [\frac{\hbar^2 k_z^2}{2m_l} + \frac{\hbar^2(k_x^2+k_y^2)}{2m_t} + (-1)^j \delta]\, I \quad [5]$$

with $\delta = \sqrt{(D\varepsilon_{xy} - \frac{\hbar^2 k_x k_y}{M})^2 + (k_x^2 + k_y^2)\Delta_{SO}^2}$, $H_3' = \left[\frac{\hbar^2 k_0 k_z}{m_l}\right] I$.

For the spin lifetime (τ) calculations, we consider the surface roughness (*SR*) and the longitudinal (*LA*) and transversal (*TA*) acoustic phonons as the prominent spin relaxation mechanisms, since the contribution of f-optical phonons can be safely neglected for a film thickness of less than 3nm. Spin and momentum relaxation rates are calculated by thermal averaging in the following way (8, 14):

$$\frac{1}{\tau} = \frac{\int \frac{1}{\tau(K_1)} f(E)(1-f(E))dK_1}{\int f(E)dK_1} \quad [6]$$

$$f(E) = \frac{1}{1+\exp(\frac{E-E_F}{K_B T})}, \int dK_1 = \int_0^{2\pi} d\emptyset \int_0^{\infty} \frac{|K_1(\emptyset,E)|}{|\frac{\partial E(K_1)}{\partial K_1}|} dE \quad [7]$$

E is the electron energy, K_1 is the in-plane wave vector, K_B is the Boltzmann constant, T is the temperature, and E_F is the Fermi level.

Surface Roughness:

The *SR*-induced spin (momentum) relaxation rate is calculated in the following way (8, 14),

$$\frac{1}{\tau_{\mathrm{SR}}(\mathrm{K}_1)} = \frac{4(2)\pi}{\hbar(2\pi)^2}\sum_{i,j}\int_0^{2\pi}\pi\Delta^2L^2\,\frac{1}{\epsilon_{ij}^2(K_2-K_1)}\,\frac{\hbar^4}{4m_l^2}\,\frac{|K_2|}{\frac{\partial E(K_2)}{\partial k_2}}\left[\left(\frac{d\varphi_{iK_{1\sigma}}}{dz}\right)^*\left(\frac{d\varphi_{jK_{2-\sigma(\sigma)}}}{dz}\right)\right]^2_{z=\pm\frac{t}{2}}\exp\left(\frac{-(K_2-K_1)^2L^2}{4}\right)d\emptyset \quad [8]$$

K_1, K_2 are the in-plane wave vectors before and after scattering, $\emptyset$ is the angle between K_1 and K_2, ϵ is the dielectric permittivity, L is the autocorrelation length, Δ is the mean square value of the surface roughness fluctuations, $\varphi_{iK_{1\sigma}}$ and $\varphi_{jK_{2\sigma}}$ are the wave functions, and σ=±1 is the spin projection to the [001] axis.

Phonons:

The electron-phonon scattering induced momentum relaxation rates are evaluated in a standard way (14). The intravalley spin relaxation due to *TA*-phonons is computed as,

$$\frac{1}{\tau_{\mathrm{TA}}(\mathrm{K}_1)} = \frac{\pi K_B T}{\hbar\rho\vartheta_{TA}^2}\sum\int_0^{2\pi}d\emptyset\,\frac{|K_2|}{\frac{\partial E(K_2)}{\partial k_2}}\left[1-\frac{\frac{\partial E(K_2)}{\partial K_2}f(E(K_2))}{\frac{\partial E(K_1)}{\partial K_1}f(E(K_1))}\right].\int_0^t\int_0^t\exp\left(-\sqrt{q_x^2+q_y^2}|z-z'|\right)\left[\varphi^\dagger_{K_2\sigma}(z)M\varphi_{K_{1-\sigma}}(z)\right]^*\left[\varphi^\dagger_{K_2\sigma}(z')M\varphi_{K_{1-\sigma}}(z')\right].\left[\sqrt{q_x^2+q_y^2}-\frac{8q_x^2q_y^2-(q_x^2+q_y^2)^2}{q_x^2+q_y^2}|z-z'|\right]dzdz' \quad [9]$$

where ρ=2329kg/m^3 is the silicon density, υ_{TA}=5300m/s is the transversal phonons velocity, t is the film thickness, (q_x, q_y)=K_1-K_2, and M written in the two valley plus two spin projection basis is

$$M=\begin{bmatrix}0 & 0 & \frac{D}{2} & 0\\ 0 & 0 & 0 & \frac{D}{2}\\ \frac{D}{2} & 0 & 0 & 0\\ 0 & \frac{D}{2} & 0 & 0\end{bmatrix}.$$

The intravalley spin relaxation rate due to the *LA*-phonons is calculated as,

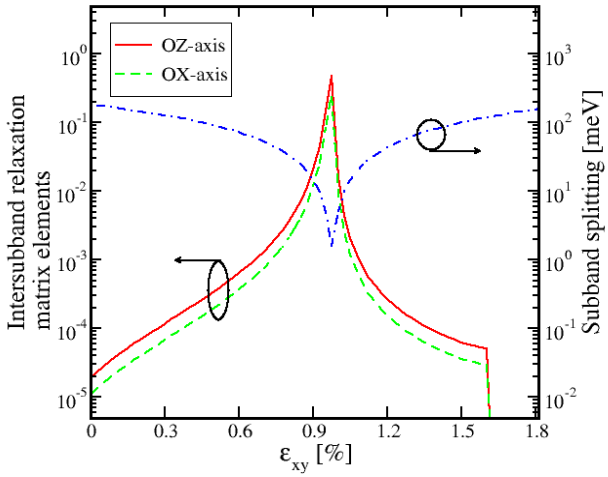

Figure 1. The intersubband *SR*-induced spin relaxation matrix elements normalized to intrasubband scattering as a function of the shear strain, when spin is injected along two different axes. The valley splitting is also shown. k_x=0.6nm^{-1}, k_y=0.7nm^{-1}, t=1.36nm.

$$\frac{1}{\tau_{\mathrm{LA}}(\mathrm{K}_1)} = \frac{\pi K_B T}{\hbar\rho\vartheta_{LA}^2}\sum\int_0^{2\pi} d\emptyset \frac{|K_2|}{\frac{\partial E(K_2)}{\partial k_2}}\left[1-\frac{\frac{\partial E(K_2)}{\partial K_2}f(E(K_2))}{\frac{\partial E(K_1)}{\partial K_1}f(E(K_1))}\right].\int_0^t\int_0^t \exp\left(-\sqrt{q_x^2+q_y^2}|z-z'|\right)\left[\varphi_{K_2\sigma}^{\dagger}(z)M\varphi_{K_{1-\sigma}}(z)\right]^*\left[\varphi_{K_2\sigma}^{\dagger}(z')M\varphi_{K_{1-\sigma}}(z')\right].\frac{4q_x^2q_y^2}{(q_x^2+q_y^2)^{3/2}}\left[\sqrt{q_x^2+q_y^2}|z-z'|+1\right]dzdz' \quad [10]$$

where v_{LA}=8700m/s is the speed of the longitudinal phonons.

The intervalley spin relaxation rate due to acoustic phonons contains the Elliot and Yafet contributions (9), and is calculated as

$$\frac{1}{\tau_{\mathrm{LA}}(\mathrm{K}_1)} = \frac{\pi K_B T}{\hbar\rho\vartheta_{LA}^2}\sum\int_0^{2\pi} d\emptyset \frac{|K_2|}{|\frac{\partial E(K_2)}{\partial k_2}|}\left[1-\frac{\frac{\partial E(K_2)}{\partial K_2}f(E(K_2))}{\frac{\partial E(K_1)}{\partial K_1}f(E(K_1))}\right].\int_0^t\left[\varphi_{K_2\sigma}^{\dagger}(z)M'\varphi_{K_{1-\sigma}}(z)\right]^*\left[\varphi_{K_2\sigma}^{\dagger}(z)M'\varphi_{K_{1-\sigma}}(z)\right].dz \quad [11]$$

where the matrix M' is:

$$M' = \begin{bmatrix} D' & 0 & 0 & D_{SO}(q_y - iq_x) \\ 0 & D' & D_{SO}(-q_y - iq_x) & 0 \\ 0 & D_{SO}(-q_y + iq_x) & D' & 0 \\ D_{SO}(q_y + iq_x) & 0 & 0 & D' \end{bmatrix}$$

with D'=12eV, D_{SO}=15meV/k_0 (9).

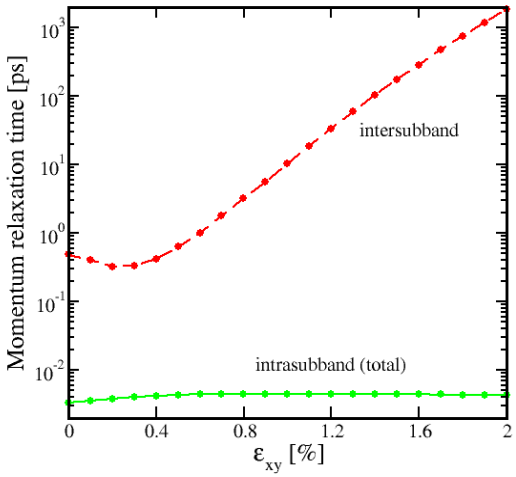

Figure 2. Variation of momentum relaxation time with stress. t=1.36nm, T=300K, N_S=10^{12}cm^{-2}.

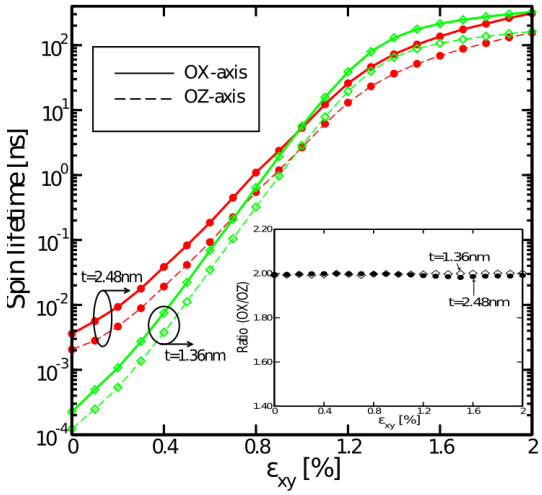

Figure 3. Spin lifetime when injected in *OX*- and *OZ*-directions. The inset shows the ratio. T=300K, N_S=10^{12}cm^{-2}.

Results and Conclusion

The surface roughness induced spin relaxation matrix elements are calculated between the wave functions with opposite spin projections (14). Figure 1 shows that the intersubband relaxation matrix elements are reduced, for an in-plane spin injection in the *OX*-direction, compared to the perpendicular-plane spin injection in the *OZ*-direction. It is further noticed that the splitting between the equivalent unprimed subbands (the valley splitting) minima and intersubband relaxation matrix elements maxima coincide.

Figure 2 shows the variation of the momentum relaxation time with stress, and indicates an increment of a factor of around two for a sample thickness of t=1.36 nm, and the electron concentration N_S=10^{12} cm^{-2}. The dominance of the intrasubband scattering process is in agreement with the selection rule that the elastic process result in strong intrasubband momentum scattering. As a sanity check we obtain that a change in spin injection direction does not influence the momentum scattering rate.

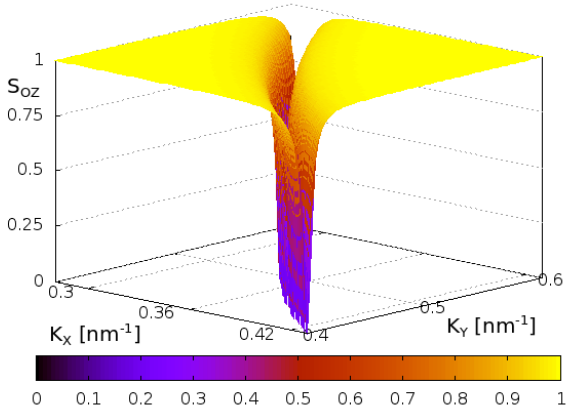

Figure 4. Total spin expectation value (S_{OZ}) for perpendicular-plane spin injection along *OZ*-axis. At the spin hotspots, S_{OZ} reaches zero. t=2.48nm, ε_{xy}=0.4%.

Figure 3 shows that under stress, the spin lifetime (τ) gets boosted by several orders of magnitude, which is a consequence of the fact that shear strain introduces the splitting between the usually considered degenerate unprimed subbands. τ is observed to be dependent of the sample thickness (t). Figure 3 also demonstrates the variation of τ when the spin injection direction is changed. We have considered an in-plane (say, *OX*-direction) and a perpendicular-plane (say, *OZ*-direction) spin injection. It is observed that the spin relaxation rate (time) decreases (increases), when spin is injected in-plane, over a wide range of applied stress. We also point out an almost constant ratio (around two) of the obtained values, for the spin injection direction sensitive τ, as shown in the inset figure. The dependence of τ on the injection direction has also been reported in bulk silicon (10).

To explain the observed increase of τ for the in-plane spin injection direction we now discuss the expectation values of the spin projection on the axes, which can be denoted as S_X, S_Y, and S_Z respectively. Consequently the total spin expectation is S_{OZ} (*OZ*-axis spin injection) or S_{OX} (*OX*-axis spin injection), where

.

$$S = \sqrt{(S_X^2 + S_Y^2 + S_Z^2)} \quad . \qquad [12]$$

The spin-orbit field (*SOF*) acts along (p_x, -p_y) direction on the *XY*-plane. In order to check S at the spin hot spots and at a fixed stress, we calculate S over a varied range of (k_x, k_y). For spin injection in *OZ*-direction we find S_X=0, S_Y=0, and S_Z also vanishes at the spin hot spots (hence S_{OZ}=0). On the contrary, when spin is injected in the in-plane *OX*-direction, we notice that at the spin hot spots

$$S_X = \sin^2(arctan\frac{p_x}{p_y}) \qquad [13a]$$

$$S_Y = -0.5\sin(2\ arctan\frac{p_x}{p_y}) \qquad [13b]$$

$$S_Z = 0 \qquad [13c]$$

and following [12],

$$S_{OX} = \sin(arctan\frac{p_x}{p_y}). \qquad [14]$$

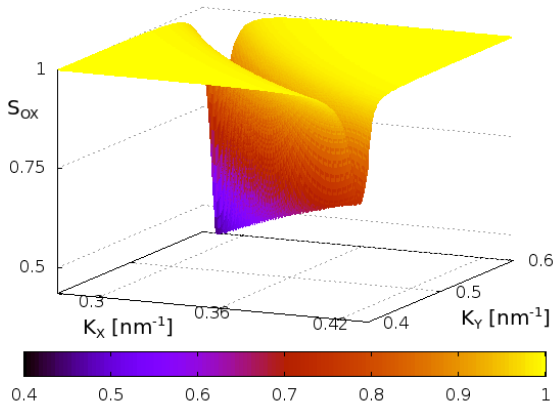

Figure 5. Total spin expectation value (S_{OX}) for in-plane spin injection along *OX*-axis. At the spin hotspots, S_{OX} [14] depends on p_x and p_y. t=2.48nm, ε_{xy}=0.4%.

Figure 4 and Figure 5 depict the variation of S_{OZ} and S_{OX} with (k_x, k_y). Due to spin precession around *SOF* lying on the XY plane, the spin projection on either axis will always be zero (non-zero), if spin is injected in perpendicular(in)-plane. Because of the zero spin expectation value at any pair of (p_x, p_y) resulting in maximal spin randomization, the spin relaxation rate (time) will be strongest (weakest) for perpendicular-plane spin injection.

Hence, our results indicate that when shear strain is applied, the momentum relaxation time can be increased by a factor of two, while the spin lifetime is boosted by orders of magnitude. The spin lifetime further increases, once spin is injected in-plane compared to perpendicular-plane.

Acknowledgments

This work is supported by the European Research Council through the grant #247056 MOSILSPIN.

References

1. D. E. Nikonov and I.A. Young, *Computer* **36**, 15 (2013).
2. J. Li and I. Appelbaum, *Phys. Rev. B* **84**, 165318 (2011).
3. S. Sugahara and J. Nitta, *Proceedings of the IEEE* **98**, 2124 (2010).
4. R. Jansen, *Nature Mat.* **11**, 400 (2012).
5. B. Huang et al., *Phys. Rev. Lett.* **99**, 177209 (2007).
6. S. P. Dash et al., *Nature* **462**, 491 (2009).
7. C. H. Li et al., *Nature Commun.* **2**, 245 (2011).
8. D. Osintsev et al., *Proc. ESSDERC*, 334 (2013).
9. Y. Song and H. Dery, *Phys. Rev.* B **86**, 085201 (2012).
10. H. Dery et al., *Appl. Phys. Lett.* **99**, 082502 (2011).
11. J. M. Tang et al., Phys. Rev. B **85**, 045202 (2012).
12. P. Li and H. Dery, *Phys. Rev. Lett.* **107**, 107203 (2011).
13. V. Sverdlov, Strain-induced effects in advanced MOSFETs, Springer 2011.
14. M. V. Fischetti et al., *J. Appl. Phys.* **94**, 1079 (2003).